THE JOURNAL OF PHYSICAL CHEMISTRY C

Article

pubs.acs.org/JPCC

pH and Temperature Modulated Aggregation of Hydrophilic Gold Nanorods with Perylene Dyes and Carbon Nanotubes

Chenming Xue,[†] Ozgul Birel,[†,‡] Yuhua Xue,[§] Liming Dai,[§] Augustine Urbas,[∥] and Quan Li*[,†]

[†]Liquid Crystal Institute, Kent State University, Kent, Ohio 44242, United States

[‡]Department of Chemistry, Mugla University, Mugla 48121, Turkey

[§]Macromolecular Science and Engineering, Case Western Reserve University, Cleveland, Ohio 44106, United States

[∥]Materials and Manufacturing Directorate, Air Force Research Laboratory, Wright-Patterson Air Force Base, Ohio 45433, United States

ABSTRACT: Hydrophilic mercaptosuccinic acid (MSA) monolayer-protected gold nanorods (GNRs) were synthesized. The resulting GNRs encapsulated with biocompatible MSA molecules via covalent Au−S linkages were found to be able to self-aggregate through intermolecular hydrogen bonding. Interestingly, when the hybrid GNRs (MSA-GNR) were mixed with the hydrophilic fluorescent perylene diimide (PDI) molecules and carboxylic acid modified single-wall carbon nanotubes (CNT-COOH), respectively, their aggregation behaviors were pH- and temperature-dependent, which were investigated by UV−vis, fluorescence spectra, and TEM images. The aggregates of MSA-GNR with functional PDI and CNT-COOH were able to combine the properties of each component through noncovalent interactions, providing insight into developing new multifunctional metal nanocomposites with properties tailored for their practical application.

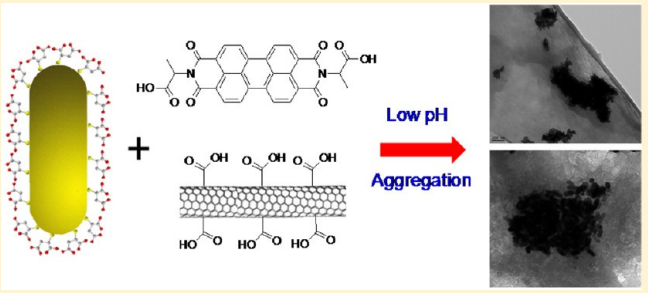

INTRODUCTION

Owing to their distinct properties compared with isotropic spherical gold nanoparticles as well as corresponding bulk materials,[1−3] anisotropic gold nanorods (GNRs) provide tremendous opportunities and challenges for insights into fundamental science which opens the doors to various applications in optics, sensing, biological imaging, and anticancer agents, etc.[4−8] Unlike isotropic spherical gold nanoparticles, GNRs have distinguishing optical properties arising from the two well-differentiated plasmon modes: transverse surface plasmon resonance (SPR) usually shows up at ∼520 nm, and longitudinal SPR appears at the near-IR region (NIR). Since GNRs respond to NIR light and have photoinduced thermal effects, they have been intensively investigated in recent years for biomedical applications, e.g., biological imaging, sensing and cancer therapy, and drug delivery.[9]

It is established that the prerequisites for GNRs' practical biomedical applications are their water solubility, biocompatibility, and in vivo stability. However, the widely investigated GNRs prepared by the seed mediated method are covered by a dynamically unstable bilayer comprising cetyltrimethylammonium bromide (CTAB) molecules,[3a] which is seemingly bioincompatible.[3c] In this context, it is of paramount importance to replace CTAB molecules on the GNR surface with hydrophilic biocompatible molecules through strong covalent Au−S linkage. Although biocompatible polymers such as polyethylene glycol (PEG) and poly(*N*-isopropylacrylamide) (PNIPAAm) were used,[10,11] small thiol-based molecules could be a promising alternative choice because of their advantages such as easy preparation and bringing of GNR in close contact to target cells or tissues to enhance the photothermal therapy effect. Small molecule mercaptosuccinic acid (MSA) is an intriguing choice because of its nontoxicity, biocompatibility, and strong hydrophilicity.[12] The thiol group in MSA molecules provides a strong covalent Au−S linkage to the GNR surface which imparts MSA covered GNRs (MSA-GNRs) with superior stability. Besides good water-solubility, the two carboxylic acid groups in the MSA molecule would also offer strong intermolecular hydrogen bonding (H-bond) to induce GNRs to consequently self-aggregate. Since different aggregation states of GNRs would result in different optical and electronic properties, it is interesting to investigate and control their aggregation behavior[13] by varying pH and temperature because the carboxylic acid groups are pH sensitive and the H-bonding is temperature sensitive.

Investigating interaction between the GNRs and other functional materials is another interesting topic because it might create novel properties of the GNRs via surface interactions and could also combine the properties of the GNRs and other functional materials together, generating new multifunctional metamaterials. Thus, interesting candidates

Received: January 23, 2013
Revised: February 25, 2013
Published: March 7, 2013

   dx.doi.org/10.1021/jp400788h | *J. Phys. Chem. C* 2013, 117, 6752−6758

such as strong fluorescent perylene diimide dyes (PDIs)[14] and carbon nanotubes (CNTs)[15,16] with superior thermal conductivity can be connected to MSA-GNR. PDIs and CNTs were also used in biomedical research. For example, PDIs were used for cell imaging[17] and as a trigger and detector for drug release[18] because of their strong fluorescence, while CNTs were used for drug delivery.[19] Here the coassembled structures of MSA-GNR with PDI, and MSA-GNR with CNT-COOH were built. The resulting coaggregated structures were able to be changed further upon modulation of pH and temperature, offering an opportunity to control aggregation with tailored functionality. The pH- and temperature-dependent aggregation of MSA-GNR, MSA-GNR with PDI, and MSA-GNR with CNT-COOH was investigated using UV−vis and fluorescence spectra and transmission electron microscopy (TEM) techniques.

EXPERIMENTAL SECTION

Materials and Measurements. All chemicals and solvents were purchased from commercial suppliers and used without further purification. $HAuCl_4$ is a 30 wt % in diluted HCl solution. UV−visible spectra were collected on a PerkinElmer Lambda 25 UV−vis spectrometer at a resolution of 1 nm. Fluorescence spectra were recorded on a FluoroMax-3 spectrofluorometer of Horiba Scientific. For transmission electron microscopy (TEM) observation, solution samples were dispersed on TEM Cu grids precoated with thin carbon film (Cu-400 CN) and thin carbon holey film (Cu-400 HN) purchased from Pacific Grid Tech. CNT was purchased from Cheap Tubes Inc.

Preparation of MSA-GNR. The CTAB-coated GNRs were freshly prepared by the seed-mediated growth method.[3a] For seed preparation, 0.5 mL of an aqueous 0.01 M solution of $HAuCl_4$ was added to CTAB solution (15 mL, 0.1 M) in a vial. A bright brown-yellow color appeared. Then 1.20 mL of 0.01 M ice-cold aqueous $NaBH_4$ solution was added all at once, followed by rapid inversion mixing for 2 min. The solution developed a pale brown-yellow color. Then the vial was kept in a water bath and maintained at 25 °C for future use. For nanorod growth, 9.5 mL of 0.1 M CTAB solution in water was added to a tube and 0.40 mL of 0.01 M $HAuCl_4$ and 0.06 mL of 0.01 M $AgNO_3$ aqueous solutions were added in this order and mixed by inversion. Then 0.06 mL of 0.1 M of ascorbic acid solution was added, and the resulting mixture at this stage becomes colorless. The seed solution (0.02 mL) was added to the above mixture tube, and the tube was slowly mixed for 10 s and left to sit still in the water bath at 25−30 °C for 3 h. The final solution turned purple within minutes after the tube was left undisturbed. The solution of CTAB-GNR was centrifuged at 7500 rpm for 20 min several times to remove the excessive CTAB and other solution components and redispersed in 1.5 mL of water. Then this aqueous solution of GNR was added dropwise to a solution of the MSA (20 mg) in 40 mL of THF with stirring. Synthesizing MSA-GNR was also reported in water.[20] The color of the reaction mixture was purple. The reaction mixture continued to stir at room temperature for 3 days and was then centrifuged. To improve the GNR with thiol molecules over the surface, the precipitates were dispersed in THF and sonicated, and then 10 mg of MSA was added to the solutions. The solution was stirred for another 24 h and centrifuged. This procedure was repeated another three times. The as-prepared GNRs were centrifuged and washed with THF several times to remove free thiols in the system.

Preparation of Water-Soluble *N,N′*-Di[(*S*)-1-carboxylethyl]-3,4,9,10-perylenetetracarboxyldiimide (PDI). PDI was synthesized according to the literature.[21] A 1 mg/mL PDI aqueous solution was made by dissolving PDI in KOH solution.

Preparation of Carboxylic Acid Modified Carbon Nanotube (CNT-COOH). An amount of 50 mg of CNT was added into a 100 mL flask containing a mixture of H_2SO_4 (30 mL, 98%) and HNO_3 (10 mL, 70%). The mixture was then ultrasonicated for 8 h. The resulting solution was diluted with 200 mL of deionized water, followed by vacuum-filtering through a 0.22 μm polycarbonate film. The solid product was washed with deionized water three times and dried to afford the CNT-COOH.

Preparation of the Solution Samples. A 0.01 M HCl aqueous solution and a 0.01 M KOH aqueous solution were prepared. For PDI solutions, PDI solid was dissolved by adding 0.01 M KOH aqueous solution. The mother solution of PDI was 1 mg/mL, pH 10. For the study of MSA-GNR aqueous solution under varied pH and temperature, the concentration of MSA-GNR was 0.1 mg/mL. For the study of MSA-GNR with PDI, the mixture was prepared by adding 1 drop of PDI mother solution into 0.1 mg/mL MSA-GNR. The concentration of PDI was approximately 2.8×10^{-6} M. For the study of MSA-GNR with CNT-COOH, the concentration of MSA-GNR was 0.1 mg/mL and the concentration of CNT-COOH was about 0.01 mg/mL.

RESULTS AND DISCUSSION

Aggregation of MSA-GNR. After thiol exchange, MSA-GNRs in THF were prepared. Since the surface of GNR was fully encapsulated by the hydrophilic carboxylic groups of MSA molecules, the as-prepared MSA-GNR was soluble in water. When dried and redissolved in water by sonication, the solution of MSA-GNRs in water displayed bluish color, which was quite different from the initial deep-red CTAB-GNR aqueous solution (Figure 1 inset). Investigating the MSA-GNRs in water is important because one potential use of the MSA-GNRs is for biomedical research. The schematic thiol exchange process is shown in Figure 2, and the UV−vis spectra of MSA-GNR, CTAB-GNR, and MSA were presented for comparison (Figure 1). For CTAB-GNR, two characteristic plasmon peaks of GNR showed up: 520 nm for the transverse SPR and 725 nm for the longitudinal SPR. After thiol exchange, the longitudinal SPR peak was at 761 nm and it became much broader. Meanwhile, there was a broadened and red-shifted transverse SPR from 520 to 535 nm. MSA molecules did not

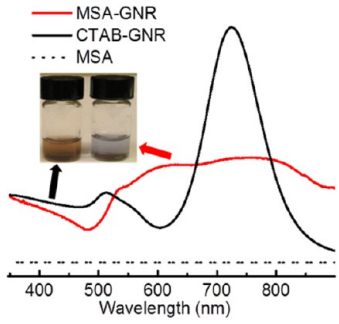

Figure 1. UV−vis spectra of CTAB-GNR, MSA-GNR, and MSA in water at room temperature. Inset: pictures of CTAB-GNR and MSA-GNR aqueous solutions.

dx.doi.org/10.1021/jp400788h | J. Phys. Chem. C 2013, 117, 6752−6758

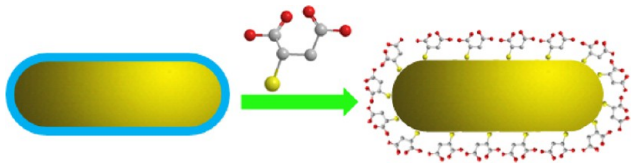

Figure 2. Preparing MSA-GNR from CTAB-GNR via thiol exchange with MSA. The hydrogen atoms of MSA molecules were omitted for clarity.

exhibit any UV signal. So the shift of the peaks could be the dielectric constant change due to the surface chemistry change after thiol exchange. The obvious broadened peak shapes indicate that there was a significant aggregation of GNRs in solution. This could be due to the intermolecular hydrogen bonding interactions offered by carboxylic groups of MSA molecules on the GNR surface. Figure 4 is the calculated

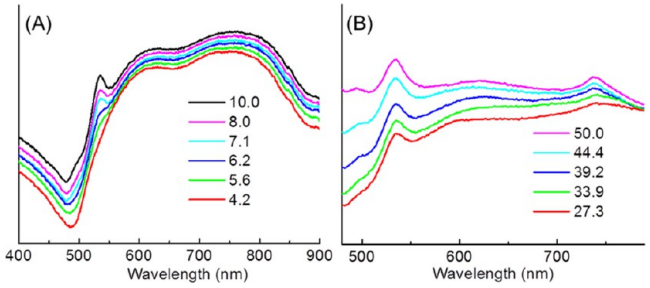

Figure 3. UV−vis spectra of MSA-GNR with (A) pH decrease at room temperature and (B) temperature increase at pH 7.

closest theoretical inter-rod distance. The shortest distance was 11.7 Å (only about 1 nm) according to the bond lengths: Au−S bond, 2.5 Å;[22] O−H 1.3 Å and S−O 1.8 Å (based on Chemdraw 3D); H-bond, 1.6−2 Å (1.8 Å was used as an average value). When base was added to the solution, the H-bond would reduce or disappear, and thus, there would be repulsive ionic interactions between MSA-GNRs, which could weaken the GNR assemblies and increase the inter-rod distance. As a result, GNR aggregation would be released. Also shown in Figure 4, MSA-GNR could connect with PDI molecules and CNT-COOH via H-bond.

With MSA molecules, the assembling behavior of the MSA-GNRs was able to be tuned by pH and temperature. Since the interparticle forces can be classified into two main categories, attractive and repulsive, MSA can provide H-bonds as the attractive force at lower pH and anionic interaction as the repulsive force at higher pH. At room temperature, the pH dependent UV−vis spectra of MSA-GNRs are shown in Figure 3A. When the pH was increased to 10 after adding KOH, the H-bond attractive force was weakened between MSA-GNRs. Ionic repulsive forces appeared between the GNRs, and the aggregations of MSA-GNRs were disassembled. When HCl was added, the pH decreased and the attractive H-bond interactions led to MSA-GNRs to aggregate. The whole process can be observed by the change of SPR peaks in the UV−vis spectra. At a high pH, the transverse SPR peak was sharp. When the pH decreased and the H-bonds became stronger, the transverse peak broadened and even disappeared at pH 4. Also, the longitudinal SPR peak endured an intensity decrease when pH decreased. The ionic repulsive interaction weakened the GNR assemblies, as reflected by the change in the transverse SPR peak shape and longitudinal peak intensity. When the pH was again increased by adding KOH, the UV−vis curves showed reversible changes. Figure 3B shows the UV−vis spectra of MSA-GNRs at pH 7 with temperature variation. Upon an increase of temperature, the assemblies of MSA-GNRs slowly degraded: both the longitudinal and the transverse SPR became sharper, particularly for the longitudinal (Figure 3B) which was not observed in Figure 3A. When the temperature cooled down, the UV−vis curves again showed reversible changes.

To corroborate the UV−vis investigation, the GNR aggregation behavior was studied by TEM. The solution samples were dropped on TEM grids and dried. For the average size based on calculating 500 GNRs, they had a length of ∼41 nm and a width of ∼15 nm. When pH increased to 10, where H-bonds were eliminated among GNRs, single GNRs appeared with large distances to other GNRs (Figure 5A). During drying some small aggregates still could be observed (Figure 5B), but the distances between GNRs were larger than those of the samples at lower pH (Figure 5C and Figure 5D) because of the ionic repulsion between carboxylate groups. When at pH 7, GNRs displayed obvious aggregation (Figure 5C). When pH further decreased to 3, there were abundant H-bond interactions between GNRs and strong aggregation of GNRs appeared (Figure 5D). Among the assemblies, side-by-side assemblies could be observed because of the large contact area along the longitudinal side between GNRs. From Figure 5B to Figure 5C and to Figure 5D, the GNR assemblies became condensed owing to the increasing H-bond interactions. Because the warm solution samples cooled during preparation

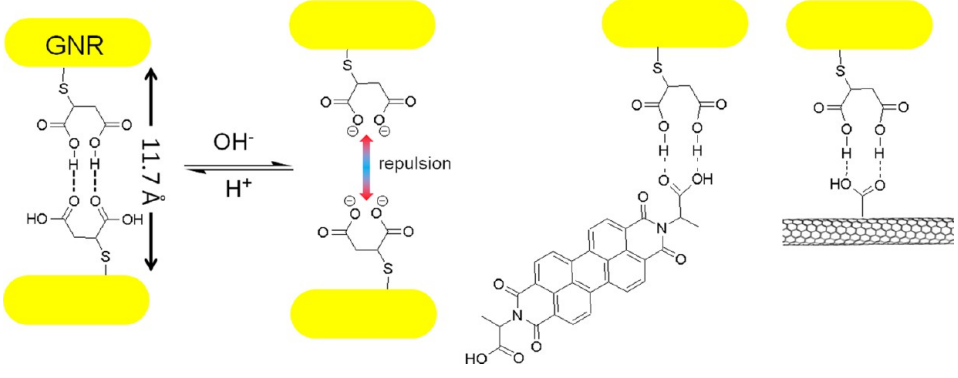

Figure 4. Schematic demonstration of interactions between MSA-GNRs provided by favoring H-bond at lower pH and electronic repulsion at higher pH, and the H-bond interactions between MSA-GNR and PDI or CNT-COOH.

dx.doi.org/10.1021/jp400788h | J. Phys. Chem. C 2013, 117, 6752−6758

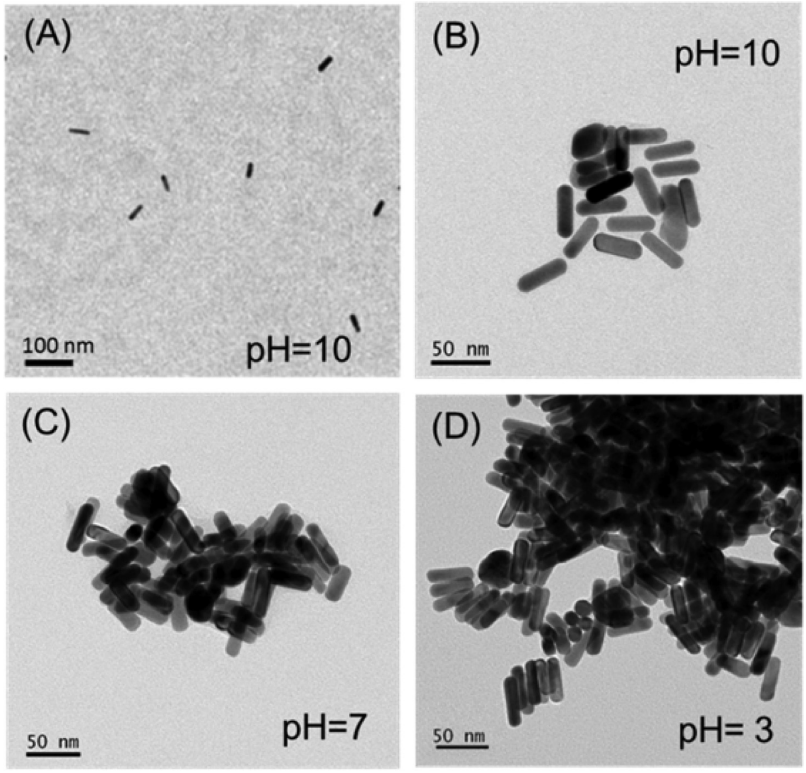

Figure 5. TEM images of MSA-GNRs drying from water solutions with different pH: (A, B) pH 10; (C) pH 7; (D) pH 3.

of TEM samples, temperature-dependent TEM studies were not shown.

Coaggregation of MSA-GNR and PDI. The aggregation behavior of MSA-GNR with other functional molecules was further investigated. Perylene molecules with carboxylic groups (PDIs) were used, which offer strong $\pi-\pi$ intermolecular interactions and H-bonds as well. With MSA and PDI, the aggregation of the GNRs could be tuned by more stimuli. First, the pH and temperature dependent UV−vis and fluorescence spectra of PDI are listed in Figure 6. The free PDI molecules exhibited two typical absorption peaks at 533 and 498 nm in the UV−vis spectra and two characteristic emission peaks at 547 and 589 nm in the fluorescence spectra. During aggregation, the intensity ratio of 533/498 in the UV−vis spectra decreased.[23,24] When aggregation became stronger, the peak at 471 nm dominated, which could usually be observed from solid-state PDI. In the fluorescence spectra, the emission intensity also decreased when the PDI assembled. At lower pH and temperature, PDI molecules tend to aggregate, displaying a lower 533/498 ratio in the UV−vis spectra (Figure 6A and Figure 6B) and a lower emission intensity in the fluorescence spectra (Figure 6C and Figure 6D). From the pH-dependent study, the PDI molecules exhibited even stronger assemblies. The absorption peak presented a shape that usually appeared in solid-state PDI, and the fluorescence peak became very weak. The pH- and temperature-dependent UV−vis and fluorescence spectra were reversible.

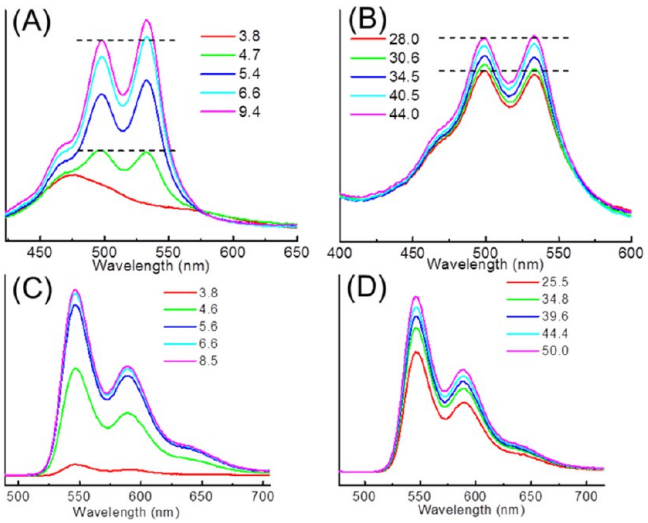

Figure 6. UV−vis spectra of PDI solution: (A) pH decrease at 28 °C; (B) temperature increase at pH 5.0. Fluorescence spectra of PDI solution: (C) pH decrease; (D) temperature increase.

The coaggregation behavior of MSA-GNRs and PDI molecules was studied. The pH dependent UV−vis and fluorescence spectra were listed in Figure 7. The pH value of the initial sample was first adjusted to 10. With the pH decrease by addition of HCl, the PDI molecule signal in the UV−vis spectra (Figure 7A) decreased and the longitudinal SPR peak of GNR further broadened and decreased in intensity, indicating that both PDI molecules and MSA-GNRs assembled. When PDI molecules were closely attached on the GNR surface, their UV−vis absorption signal could not be observed.[25] When they were no longer assembled on the GNR surface, their signal reappeared. In the fluorescence spectra in Figure 7C, the intensity of the PDI molecules was reduced, similar to Figure 6C. Conversely, during the pH increase the PDI molecules released from the assemblies and the characteristic absorption and fluorescence peaks increased (Figure 7B and Figure 7D). The longitudinal SPR peak also slightly increased, but it was not as obvious as in the initial state at pH 10.4 in Figure 7A.

dx.doi.org/10.1021/jp400788h | J. Phys. Chem. C 2013, 117, 6752−6758

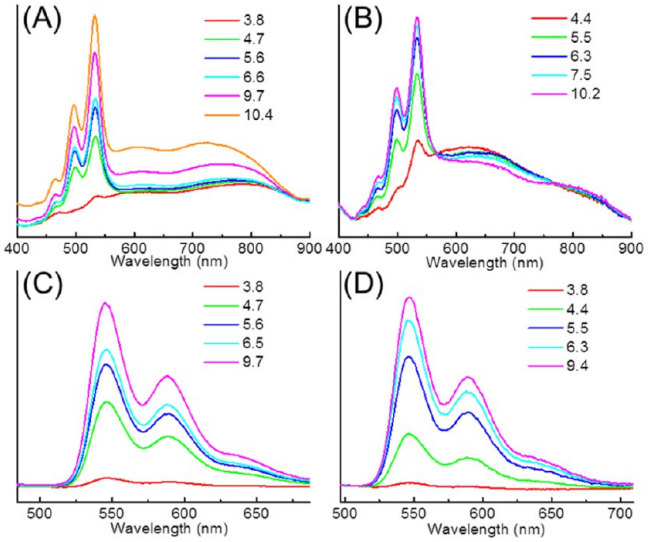

Figure 7. UV−vis spectra of the MSA-GNRs and PDI mixed solution at 28 °C under (A) pH decrease and (B) pH increase. Corresponding fluorescence spectra: (C) pH decrease and (D) pH increase.

This indicated that the coaggregation of MSA-GNR with PDI was easy to disassemble. Different from PDI molecules, the coaggregation did not generate PDI aggregation as strong as in Figure 7A at around pH 4. This could be ascribed to the coaggregation of MSA-GNRs and PDI molecules, rendering the formation of highly ordered PDI assemblies.

The temperature-dependent UV and fluorescence spectra are shown in Figure 8. During the temperature increase, as shown

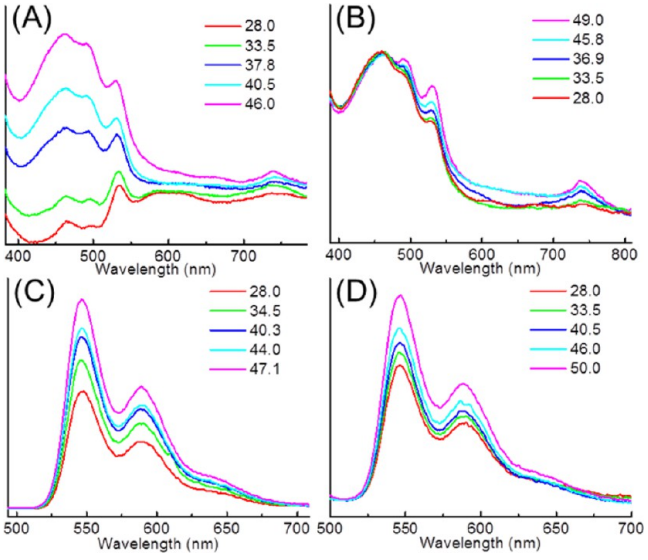

Figure 8. UV−vis spectra of the MSA-GNRs and PDI coaggregation in solution at pH 4 under increasing (A) and decreasing (B) temperatures. Bottom: corresponding fluorescence spectra.

in Figure 8A, the absorption peaks corresponding to the PDI molecules increased. The typical PDI UV−vis absorption peaks indicate highly self-assembled PDI molecules in all temperature variations. There was also an accompanying change of the MSA-GNRs' longitudinal SPR peak. Both sharpness and intensity increased, indicating the loss of the MSA-GNRs assemblies. The fluorescence peak intensity also increased in Figure 8C during heating. The increase trend was not as strong as from free PDI molecules because they were aggregated at low pH. During cooling as shown in Figure 8B, PDI molecules did not show obvious changes in UV−vis spectra; nevertheless, the change of the MSA-GNRs' longitudinal SPR peaks seemed to exhibit reversible behavior (compared to Figure 8A). The fluorescence spectra during cooling also exhibited a slower intensity decrease compared to free PDI. The separation of MSA-GNRs and PDI assemblies from the coaggregation structure could be the reason to explain the above observations. During heating, the H-bond interactions between MSA-GNRs and MSA-GNRs, MSA-GNRs and PDI became weaker but the $\pi-\pi$ interactions of PDI molecules were still very strong. Therefore, the MSA-GNR-PDI coassemblies disassembled. MSA-GNR aggregates further disassembled, but the separated PDI assemblies remained. During cooling, the MSA-GNRs assembled and the longitudinal peak became broader and weaker. However, the absorption peak of PDI aggregates remained indicating that PDI aggregates did not coassemble with MSA-GNRs the same way as its initial state. The temperature dependent study showed an irreversible change of MSA-GNRs and PDI coaggregations.

For the pH-dependent study, the TEM images of MSA-GNRs and PDI assemblies were also illustrated in Figure 9. The

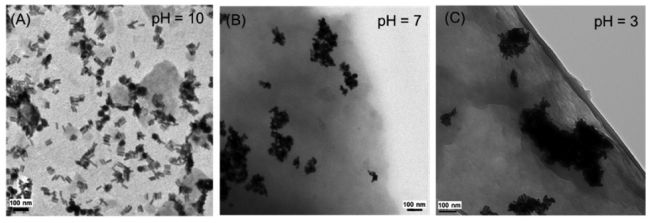

Figure 9. TEM images of MSA-GNR-PDI drying from water solutions with different pH values: (A) pH 10; (B) pH 7; (C) pH 3.

increasing trend of forming aggregation when pH decreased could be clearly observed. At pH 10 (Figure 9A), there were no H-bond interactions between MSA-GNRs and PDI. The MSA-GNRs showed a good dispersion where individual GNRs without aggregation or a few GNRs presenting weak aggregates could be observed. For PDI molecules at high pH, PDI molecules still could aggregate based on strong $\pi-\pi$ interactions during drying. At pH 7, there were H-bond attractive interactions, so the two components aggregated and formed coassemblies, as shown in Figure 10B. By further adjustment of the pH to 3 (Figure 10C), even larger aggregates of MSA-GNR were exhibited in the coaggregation structure, according to the stronger H-bond interactions among GNRs.

Coaggregation of MSA-GNR and Carboxylic Acid Modified Carbon Nanotubes (CNT-COOH). Although GNRs were used for their photothermal effect, this effect only took place near the GNRs. By mixing of GNRs into CNT networks, with superior thermal conductivity of CNT,[26] the photothermal effect of GNRs could be further enhanced by including a larger area. In this work strong H-bonded MSA-GNRs and CNT-COOH were combined. As the CNTs had a strong absorption at about 260 nm in UV−vis spectra, there was no overlap of signals between the GNRs and the CNTs in that region. However, CNTs still have some weak absorption in the UV−vis−NIR region.[27] In our experiment, the CNT solution samples before and after adding MSA-GNR were compared as shown in Figure 10A. Clearly, after addition of MSA-GNR, a much stronger peak at 574 nm appeared, and the

dx.doi.org/10.1021/jp400788h | J. Phys. Chem. C 2013, 117, 6752−6758

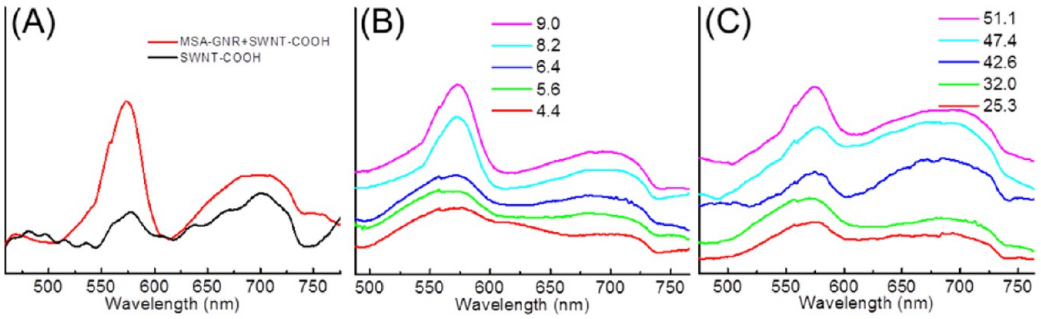

Figure 10. UV−vis spectra of MSA-GNRs mixing with CNT-COOH at pH 4 (A) and their further studies with pH decrease (B) and temperature increase (C).

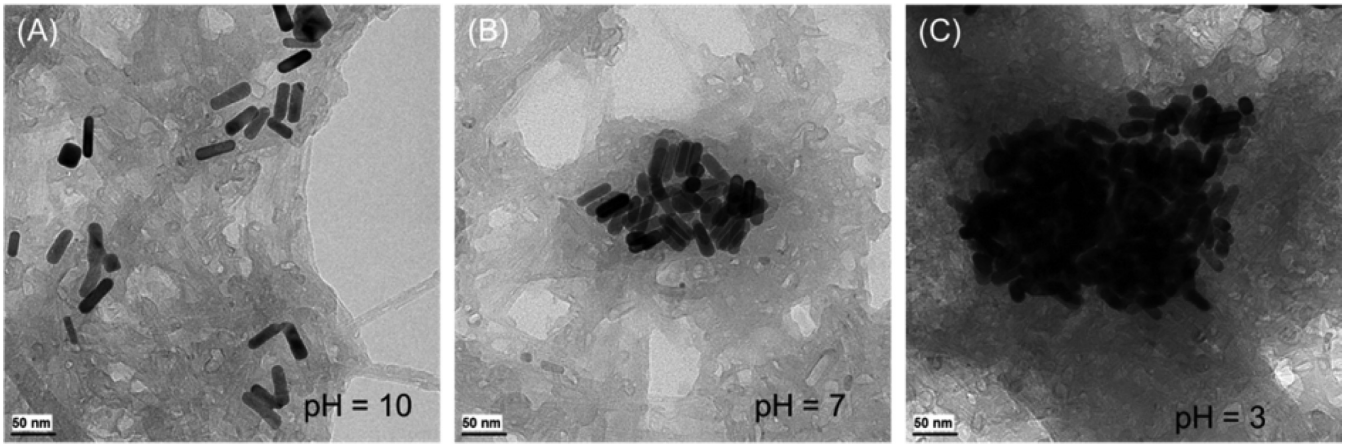

Figure 11. TEM images of MSA-GNR-CNT-COOH drying from water solutions with different pH: (A) pH 10; (B) pH 7; (C) pH 3.

peak at 705 nm became broader and had higher intensity. This indicates that the MSA-GNRs presented their characteristic absorption when mixing with CNTs in aqueous solution. Different from the 535 and 761 nm SPR peaks of initial MSA-GNRs in Figure 1, the new SPR peaks of the MSA-GNRs mixed with CNTs could be ascribed to the influence of the CNTs which may alter the effective dielectric constant of the coating layer on the GNR when attached onto the GNR surface. For the mixture, the pH- and temperature-dependent UV−vis spectra were presented in Figure 10B and Figure 10C. Similar to the MSA-GNR sample, the mixture exhibited strong assemblies of GNRs at lower pH and temperature and exhibited weaker assemblies at higher pH and temperature by showing peak changes in shape and intensity at 574 and 705 nm. With H-bond interactions between CNT-COOH and MSA-GNR, the GNR could be dispersed and stabilized in CNT networks. Both of the UV spectra had reversible changes when pH and temperature were adjusted back.

The aggregations could also be observed by TEM as shown in Figure 11. When at pH 10, the MSA-GNRs could disperse in CNT networks. When the pH was decreased to 7 and further to 3, GNR assemblies formed and became larger and more condensed. By comparison to Figure 11A and Figure 11B, the CNT networks in Figure 11C also turned out to be more condensed, since CNT-COOH tended to aggregate via H-bonds as well. In addition, Figure 11 indicates MSA-GNR had a stronger tendency to self-aggregate than to disperse and coassemble with CNT-COOH when pH decreased.

On the basis of the UV−vis spectra and TEM images, the MSA-GNRs with other functional materials such as fluorescent perylene diimide dye molecules and carbon nanotubes are depicted in Figure 12. During pH decrease and increase, MSA-GNRs in all these samples could correspondingly assemble and disassemble, reflected by the changes of the characteristic longitudinal and transverse SPR peaks. Because of the H-bond interactions when the pH decreased, the MSA-GNRs aggregated, and the PDI or CNT-COOH would coaggregate with the MSA-GNRs. When the pH increased, the H-bond

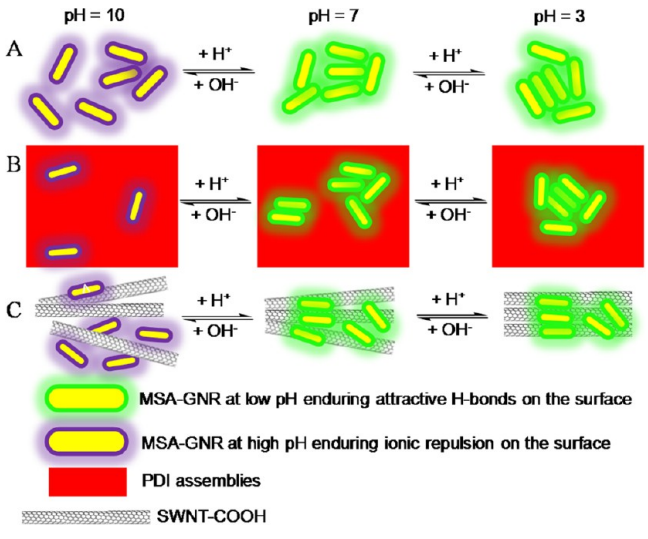

Figure 12. Schematic description of GNR aggregation behavior under varied pH values: (A) MSA-GNR; (B) MSA-GNR with PDI; (C) MSA-GNR with CNT-COOH. The carboxylic groups on CNT-COOH were omitted for clarity.

dx.doi.org/10.1021/jp400788h | J. Phys. Chem. C 2013, 117, 6752−6758

effect would decrease and instead the electronic repulsive interactions of the carboxylate ion groups appeared, preventing the MSA-GNRs from forming assemblies. For the MSA-GNRs only, besides individual GNRs, small weak aggregates still existed during drying but the distances between the GNRs increased because of ionic repulsive interactions. For PDI molecules with strong $\pi-\pi$ interactions, they still could assemble during drying. But owing to the lack of attractive H-bond interactions between MSA-GNRs, MSA-GNRs in the free-state or with weak aggregates formed assembling with PDI. For GNRs mixing with CNT-COOH, both of the CNTs and the GNRs would disassemble. From the temperature-dependent study, an interesting discovery of MSA-GNRs mixing with PDI could be observed. From the UV−vis spectra, there were irreversible changes during heating and cooling. This was because of the strong $\pi-\pi$ interactions between PDI molecules that prevented them from disassembling and mixing with the GNRs during cooling. For the MSA-GNRs and the MSA-GNRs mixing with CNT-COOH, there were reversible coaggregations during heating and cooling.

CONCLUSIONS

In summary, the coaggregation behaviors of biocompatible MSA-covered GNRs and their mixtures with functional materials such as perylene dye and carbon nanotubes based on hydrogen bonding were investigated. Their pH- and temperature-dependent aggregation behavior was studied by UV−vis, fluorescence spectra, and TEM images. There are several potential advantages of these materials. First, the hydrophilic GNRs covered by biocompatible, small MSA molecules could increase the photothermal effect with shorter distances between GNRs and the contacting area. In addition, by manipulation of the SPR absorption peaks with the pH and temperature controlled assembled structures, the activation light can be tuned and even shifted more into the NIR region. Introducing PDI molecules and CNT networks to GNRs could bring multifunction such as bioimaging and modified thermal conduction properties. This research on aggregation behavior of multifunctional nanostructures containing multiple components through intermolecular noncovalent interactions provides new insight into the development of novel multifunctional metal nanocomposites.

AUTHOR INFORMATION

Notes

The authors declare no competing financial interest.

ACKNOWLEDGMENTS

This work was supported by the Air Force Office of Scientific Research (Grant AFOSR FA9550-09-1-0254). Support from AFOSR-MURI (Grant FA9550-12-1-0037) and TUBITAK (Grant 2219) from Turkey is also acknowledged. The TEM data were obtained with assistance from Min Gao at the (cryo) TEM facility at the Liquid Crystal Institute, Kent State University, OH, supported by the Ohio Research Scholars Program Research Cluster on Surfaces in Advanced Materials.

REFERENCES

(1) Daniel, M. C.; Astruc, D. *Chem. Rev.* **2004**, *104*, 293−346.
(2) Halas, N. J.; Lal, S.; Chang, W. S.; Link, S.; Nordlander, P. *Chem. Rev.* **2011**, *111*, 3913−3961.
(3) (a) Sau, T. K.; Murphy, C. J. *Langmuir* **2004**, *20*, 6414−6420. (b) Murphy, C. J.; San, T. K.; Gole, A. M.; Orendorff, C. J.; Gao, J. X.; Gou, L.; Hunyadi, S. E.; Li, T. *J. Phys. Chem. B* **2005**, *109*, 13857−13870. (c) Niidome, T.; Yamagata, M.; Okamoto, Y.; Akiyama, Y.; Takahashi, H.; Kawano, T.; Katayama, Y.; Niidome, Y. *J. Controlled Release* **2006**, *114*, 343−347.
(4) Nikoobakht, B.; Wang, J. P.; El-Sayed, M. A. *Chem. Phys. Lett.* **2002**, *366*, 17−23.
(5) Yu, C. X.; Irudayaraj, J. *Anal. Chem.* **2007**, *79*, 572−579.
(6) Pissuwan, D.; Valenzuela, S. M.; Miller, C. M.; Cortie, M. B. *Nano Lett.* **2007**, *7*, 3808−3812.
(7) Norman, R. S.; Stone, J. W.; Gole, A.; Murphy, C. J.; Sabo-Attwood, T. L. *Nano Lett.* **2008**, *8*, 302−306.
(8) Vigderman, L.; Khanal, B.; Zubarev, E. R. *Adv. Mater.* **2012**, *24*, 4811−4841.
(9) Huang, X.; Neretina, S.; El-Sayed, M. A. *Adv. Mater.* **2009**, *21*, 4880−4910.
(10) Choi, J.; Yang, J.; Bang, D.; Park, J.; Suh, J. S.; Huh, Y. M.; Haam, S. *Small* **2012**, *8*, 746−753.
(11) Shiotani, A.; Mori, T.; Niidome, T.; Niidome, Y.; Katayama, Y. *Langmuir* **2007**, *23*, 4012−4018.
(12) Ying, E.; Li, D.; Guo, S.; Dong, S.; Wang, J. *PloS One* **2008**, *3*, e2222.
(13) Romo-Herrera, J. M.; Alvarez-Puebla, R. A.; Liz-Marzan, L. M. *Nanoscale* **2011**, *3*, 1304−1315.
(14) Würthner, F. *Chem. Commun.* **2004**, 1564−1579.
(15) Tans, S. J.; Devoret, M. H.; Dai, H. J.; Thess, A.; Smalley, R. E.; Geerligs, L. J.; Dekker, C. *Nature* **1997**, *386*, 474−477.
(16) Schnorr, J. M.; Swager, T. M. *Chem. Mater.* **2011**, *23*, 646−657.
(17) Liu, H. M.; Wang, Y. L.; Liu, C. H.; Li, H. X.; Gao, B. X.; Zhang, L. C.; Bo, F. L.; Bai, Q. Q.; Ba, X. W. *J. Mater. Chem.* **2012**, *22*, 6176−6181.
(18) Jana, A.; Devi, K. S. P.; Maiti, T. K.; Singh, N. D. P. *J. Am. Chem. Soc.* **2012**, *134*, 7656−7659.
(19) Ilbasmis-Tamer, S.; Yilmaz, S.; Banoglu, E.; Degim, I. T. *J. Biomed. Nanotechnol.* **2010**, *6*, 20−27.
(20) Dai, Q.; Coutts, J.; Zou, J. H.; Huo, Q. *Chem. Commun.* **2008**, 2858−2860.
(21) Xu, T.; Leng, S.; Xue, C.; Sun, R.; Pan, J.; Ford, J.; Jin, S. *Angew. Chem., Int. Ed.* **2007**, *46*, 3896−3899.
(22) Cossaro, A.; Mazzarello, R.; Rousseau, R.; Casalis, L.; Verdini, A.; Kohlmeyer, A.; Floreano, L.; Scandolo, S.; Morgante, A.; Klein, M. L.; Scoles, G. *Science* **2008**, *321*, 943−946.
(23) Wang, W.; Han, J. J.; Wang, L. Q.; Li, L. S.; Shaw, W. J.; Li, A. D. Q. *Nano Lett.* **2003**, *3*, 455−458.
(24) Xue, C. M.; Chen, M. Z.; Jin, S. *Polymer* **2008**, *49*, 5314−5321.
(25) Xue, C. M.; Birel, O.; Gao, M.; Zhang, S.; Dai, L. M.; Urbas, A.; Li, Q. *J. Phys. Chem. C* **2012**, *116*, 10396−10404.
(26) Ren, C. L.; Zhang, W.; Xu, Z. J.; Zhu, Z. Y.; Huai, P. *J. Phys. Chem. C* **2010**, *114*, 5786−5791.
(27) Ryabenko, A. G.; Dorofeeva, T. V.; Zvereva, G. I. *Carbon* **2004**, *42*, 1523−1535.